A hybrid continuous-discrete nonlinear observer for real-time SOC estimation for Supercapacitor

I. Belghazi[1] and E. Magarotto[2,*] and T. Ahmed-Ali [3] and P. Dorléans [2] and M. Haddad [5]

***Abstract*— In this paper, an online method for estimating the internal voltages of SuperCapacitors (SCs) is proposed, based on two- and three-branch models. The primary goal is to deliver fast and accurate real-time voltage estimation, which is essential for assessing the State of Charge (SOC). A hybrid nonlinear observer is designed to estimate voltages using only sampled measurements. The proposed approach explicitly exploits the distinct time constants of each branch, enabling a clear separation between fast and slow dynamics and facilitating the stability analysis. In addition, the observer incorporates a correction term during the prediction step, allowing continuous state updates between sampling instants and improving estimation accuracy even for large sampling periods. This makes the method suitable for efficient real-time implementation. Simulation results demonstrate the effectiveness of the proposed observer for SOC estimation using the three-branch (3B) model, particularly under highly dynamic input profiles such as the Worldwide Harmonized Light Vehicle Test Procedure (WLTP).**

***Index Terms*— Nonlinear, Observer, Sampled-data, Lyapunov, Supercapacitor, State of Charge, WLTP.**

I. Introduction

Accurate estimation of SOC is a critical issue in the management of Energy Storage Systems (ESS), particularly in applications such as Electric Vehicles (EVs) and embedded systems operating under fast and highly dynamic conditions [1]. In this context, SCs have attracted significant interest due to their high power density, fast charge-discharge capability, and long cycle life [2]. When combined with batteries, SCs contribute to improving energy efficiency, enhancing regenerative braking performance, and reducing battery degradation, thereby improving the overall system lifetime [3], [4]. The performance of such hybrid energy storage systems strongly depends on the availability of reliable SOC estimation methods capable of operating under realistic sampling and implementation constraints [5], [6]. Observer-based approaches are widely used to estimate internal states from measurable signals such as current and terminal voltage. Among the available modeling approaches, equivalent circuit models (ECMs) provide a good compromise between accuracy and computational complexity. While one and two-branch (2B) models are often preferred for their simplicity, they fail to fully capture the multi-time-scale internal dynamics of SCs [7], [8]. In contrast, 3B models introduce additional time constants, allowing a more accurate representation of both fast and slow dynamics, which is particularly relevant for advanced observer design [9].

Various observer-based techniques have been proposed in the literature for SOC estimation. Classical approaches include Luenberger observers [10], while more advanced methods rely on Kalman filtering techniques such as the Extended Kalman Filter (EKF) and Unscented Kalman Filter (UKF) [11], [12]. Nonlinear observers, including high-gain observers and generalized extended state observers, have also been investigated to improve robustness and convergence properties [13], [14]. Although these methods generally provide satisfactory performance, their implementation in real-time embedded systems remains challenging due to computational constraints and sensitivity to sampling effects. To address these issues, sampled-data observers have been widely considered, as they are naturally suited for digital implementation [15]. A common approach relies on Zero-Order-Hold (ZOH) assumptions, where the output is considered constant between two sampling instants. While this approach simplifies implementation and reduces computational cost, it neglects the continuous evolution of the system between sampling instants, which may lead to degraded estimation accuracy under fast dynamics or large sampling periods.

In our previous work [16], a nonlinear sampled observer based on a ZOH strategy was proposed for a 3B SC model and validated under realistic cycles such as New European Driving cycle (NEDC) and WLTP. Despite its satisfactory performance, the ZOH approximation remains a limiting factor in accurately capturing inter-sample behavior.

To overcome these limitations, this paper proposes a hybrid continuous-discrete nonlinear observer with inter-sample output prediction. Unlike classical sampled observers, the proposed approach explicitly accounts for the system evolution between sampling instants by introducing a continuous correction mechanism during the prediction phase. This feature significantly improves estimation accuracy while preserving compatibility with digital implementation. Furthermore, the observer design exploits the separation of time scales inherent to the 3B model, which facilitates stability analysis and enhances robustness under fast-varying operating conditions.

Compared to existing approaches in the literature, the main contribution of this work lies in the integration of the inter-sample prediction within a nonlinear observer frame-

[1]IRSEEM, 76000 Rouen and SEGULA Engineering, SEGULA Technologies, 92 500 Rueil Malmaison, France;

[2]Université Caen Normandie, Normandie Univ, LSEM UR 7484, 14000 Caen, France;

[*] corresponding author : eric.magarotto@unicaen.fr

[3]ENSICAEN & Université Caen Normandie, Normandie Univ, LSEM UR 7484, 14000 Caen, France

[5]head of R&I Department - SEGULA Engineering, SEGULA Technologies, 9 av. E. Belin, 92 500 Rueil Malmaison, France

work, providing an effective compromise between estimation accuracy and computational complexity. In particular, the proposed method extends classical ZOH-based observers by incorporating continuous-time correction, resulting in improved performance without significantly increasing implementation cost. Similar challenges related to real-time optimization and energy management in electrical systems have also been addressed in [17].

The remainder of this paper is organized as follows: Section II presents the SC model. Section III details the hybrid nonlinear observer design and its stability properties. Simulation results and comparative analyses are discussed in Section IV, before concluding remarks are presented in the final Section.

II. SUPERCAPACITOR CIRCUIT MODEL

A. Model discussion

SCs are commonly modeled using ECMs. Depending on the desired level of accuracy, several structures can be considered. The simplest model, based on a single RC branch, is typically provided by manufacturers and is mainly suitable for basic applications. However, it neglects important phenomena such as charge redistribution and the dependence of capacitance on voltage.

To capture more complex behaviors, multi-branch models such as 2B and 3B configurations are widely used. The 2B model introduces fast and slow dynamics associated with charge storage and redistribution effects. The 3B model further improves this representation by incorporating an additional intermediate time constant, allowing a more accurate description of the internal dynamics of the SC.

Although higher-order models (four branches or more) can provide a better fit to Electrochemical Impedance Spectroscopy (EIS) data, they significantly increase the number of parameters to be identified and the computational burden, while providing only marginal improvements in estimation accuracy (typically less than 1%) [18]. Therefore, the 3B model represents a suitable compromise between model accuracy and implementation complexity for real-time SOC estimation .

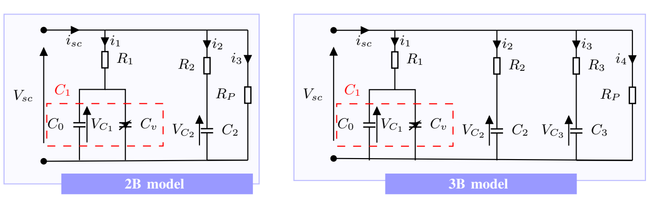

Fig. 1. Supercapacitor models

B. Model equations

The 2B and 3B models are illustrated in Fig. 1. In these configurations, V_{sc} denotes the terminal voltage of the SC, and i_{sc} is the input current (i.e., $u(t) = i_{sc}(t)$). The variables V_{C_k}, $k = 1, 2, 3$, denote the internal voltages across each RC branch. The resistances R_k correspond to the branch resistances, R_p is the leakage resistance, and R_{eq} is the equivalent series resistance. The capacitances C_k are associated with the dynamic branches of the SC.

In this model, the first branch capacitance C_1 is considered voltage-dependent in order to capture the nonlinear behavior of the SC. This dependency reflects the physical characteristics of electrochemical double-layer capacitors, where the capacitance varies with voltage due to charge distribution mechanisms at the electrode interface. The capacitance is approximated by a first-order nonlinear function of the internal voltage V_{C_1} in $C_1 = g(V_{C_1}) = C_0 + C_v V_{C_1}$ which plays a key role in capturing the real performance of the SC, particularly under varying voltage conditions. Note that you can find some works using the second order approximation of C_1.

C. State-space formulation

1) Three-branch model: Applying Kirchhoff current and voltage laws, and defining the state vector $X^T = [V_{C_1}\ V_{C_2}\ V_{C_3}]$, the system can be written as (with $C_1 = C_0 + C_v X_1$):

$$\begin{cases} \dot{X}(t) & = A_{3b}\ X(t) + B_{3b}\ u(t) = \phi\left(X(t), u(t)\right) \\ Y(t) & = C_{3b}\ X(t) + D\ u(t) \end{cases} \tag{1}$$

where $Y(t) = V_{SC}(t)$ is the measured output. The matrices A_{3b} and B_{3b} depend on the state through the capacitance C_1, which makes the system nonlinear. Although the structure may appear linear, the dependence of the time constant $\tau_1 = R_1 C_1$ on the state introduces a nonlinear behavior.

$$A_{3b} = \begin{bmatrix} A_{11} A_{12} A_{13} \\ A_{21} A_{22} A_{23} \\ A_{31} A_{32} A_{33} \end{bmatrix} = \begin{bmatrix} \frac{(R_{eq}-R_1)}{R_1\tau_1} & \frac{R_{eq}}{R_2\tau_1} & \frac{R_{eq}}{R_3\tau_1} \\ \frac{R_{eq}}{R_1\tau_2} & \frac{(R_{eq}-R_2)}{R_2\tau_2} & \frac{R_{eq}}{R_3\tau_2} \\ \frac{R_{eq}}{R_1\tau_3} & \frac{R_{eq}}{R_2\tau_3} & \frac{(R_{eq}-R_3)}{R_3\tau_3} \end{bmatrix}$$

$$B_{3b}^T = \begin{bmatrix} B_1 & B_2 & B_3 \end{bmatrix}, C_{3b} = \begin{bmatrix} C_1 & C_2 & C_3 \end{bmatrix}, D = R_{eq}$$

where $B_i = \frac{R_{eq}}{\tau_i}$ and $C_i = \frac{R_{eq}}{R_i}$ with $\tau_i = R_i C_i$, $i = 1, 2, 3$.

The 2B model can be obtained from the 3B formulation by removing the third RC branch associated with the intermediate dynamics.

III. HYBRID NONLINEAR OBSERVER WITH OUTPUT PREDICTION

In previous work [16], a continuous-time nonlinear observer was proposed for a 3B SC model. The system was decoupled into two subsystems: a nonlinear part associated with fast dynamics, and a linear part describing intermediate and slow dynamics. A sampled-data observer based on a ZOH strategy was also developed and validated under various cycles such as NEDC and WLTP.

Although the ZOH-based observer provided satisfactory estimation performance, it assumes that the output remains constant between two sampling instants. This approximation neglects the continuous evolution of the system and may lead to degraded estimation accuracy under fast-varying inputs or large sampling periods.

To overcome this limitation, we now propose a hybrid continuous-discrete nonlinear observer with inter-sample output prediction. The key idea is to combine continuous-time state estimation with discrete-time measurement updates. Between sampling instants, the observer evolves continuously using a prediction of the output, while at each sampling instant, it is corrected using the available measurement. This structure allows improving estimation accuracy while preserving compatibility with real-time digital implementation.

Here, we apply the hybrid observer to both the 2B and 3B SC models, with the aim of comparing their real-time SOC estimation. This comparative study will highlight the advantages of using 3B model, showing that it provides superior estimation accuracy under realistic and demanding load profiles, while maintaining compatibility with embedded system constraints.

A. Continuous-time observer

1) observability: To analyze local observability, we use the Lie derivative-based rank condition for nonlinear systems. As the input is measurable and known, the term $(D\ u)$ can be subtracted from the output y ,leading to an equivalent output function $h(x)$.

The observability matrix is then defined as : $\mathcal{O}(X) = \begin{bmatrix}\frac{\partial h(x)}{\partial x} & \frac{\partial L_f h(x)}{\partial x} & \frac{\partial L_f^2 h(x)}{\partial x}\end{bmatrix}^T = \begin{bmatrix}C & CA_{3b} & CA_{3b}^2\end{bmatrix}^T$. The observability matrix has full rank equal to 3, which proves that the system is locally observable.

2) continuous observer synthesis: Let $X^T = [X_1\ Z]$ and define $\phi_1 = [A_{11}\quad A_{12}\quad A_{13}]X + B_1\ u$, then the system (1) can be expressed under the following form:

$$\begin{cases} \dot{X}_1(t) &= \phi_1\ \ (X(t), u(t)) \\ \dot{Z}(t) &= \bar{A}Z(t) + \bar{\bar{A}}\ X_1(t) + \bar{B}\ u(t) \\ Y(t) &= C_1 X_1(t) + \bar{C}\ Z(t) + Du(t) \end{cases} \tag{2}$$

with ϕ_1 a nonlinear function of X_1 and $Z^T = [X_2\ X_3]$ the linear part with $\bar{A} = \begin{bmatrix} A_{22} & A_{23} \\ A_{32} & A_{33}\end{bmatrix}$, $\bar{\bar{A}} = \begin{bmatrix} A_{21} \\ A_{31}\end{bmatrix}$, $\bar{B} = \begin{bmatrix} B_2 \\ B_3\end{bmatrix}$ and the output with $\bar{C} = \begin{bmatrix} C_2 & C_3\end{bmatrix}$.

The choice of this structure lies in the fact that we want to separate linear and nonlinear parts in order to treat entirely the linear part of this system with global gain. This approach differs from [14] where each observer gain act only on each respective state without taking account of the other.

We introduce the following hypothesis :

Hypothesis 1: We suppose that the control input signal is bounded and ϕ_1 is locally Lipschitz with constant σ.

Based on (1), and assuming continuous availability of the output, the following continuous-time observer is proposed:

$$\begin{cases} \dot{\hat{X}}_1(t) = \phi_1(\hat{X}(t), u(t)) + l_1\,(y(t) - \hat{y}(t)) \\ \dot{\hat{Z}}(t) = \bar{A}\hat{Z}(t) + \bar{\bar{A}}\hat{X}_1(t) + \bar{B}u(t) + L\,(y(t) - \hat{y}(t)) \\ \hat{Y}(t) = C_1\hat{X}_1(t) + \bar{C}\ \hat{Z}(t) + Du(t) \end{cases} \tag{3}$$

and $L^T = [l_2\ l_3]$ with l_1, l_2 and l_3 positive gains of this observer.

3) Computation of gains: The gain matrix L is determined by placing the eigenvalues of the matrix $(\bar{A} + L\bar{C})$ in the left half-plane. The gains l_1, L must also satisfy constraints derived from Lyapunov stability analysis and Young's inequality.

Theorem 3.1: There exists l_1 and a gain vector L such that the continuous observer (3) is exponentially convergent under Hypothesis 1.

Sketch of Proof:

Omitting (t) for the sake of simplicity, let us define $\tilde{Z} = Z - \hat{Z}, \tilde{X}_1 = X_1 - \hat{X}_1, X^T = [X_1\ Z], \tilde{X}^T = [\tilde{X}_1\ \tilde{Z}]$. The error dynamics are given by:

$$\dot{\tilde{X}}_1 = \phi_1(\hat{X}, u) - \phi_1(X, u) - l_1 C_1 \tilde{X}_1 - l_1 \bar{C}\tilde{Z} \tag{4}$$

$$\dot{\tilde{Z}} = (\bar{A} - L\bar{C})\tilde{Z} + (\bar{\bar{A}} - LC_1)\ \tilde{X}_1 \tag{5}$$

Define a Lyapunov candidate function as:

$$V = V_1 + V_2 = \frac{1}{2}\tilde{X}_1^2 + \tilde{Z}^T P\ \tilde{Z} \tag{6}$$

The matrix P must satisfy the Lyapunov inequality :

$$P(\bar{A} - L\bar{C}) + (\bar{A} - L\bar{C})^T P \leqslant -\mu I, \qquad \mu > 0 \tag{7}$$

Then, using Young's inequality and after some manipulations,

$$\dot{V}_1 \leqslant \left(\sigma - l_1\frac{C_1}{2}\right)\ |\tilde{X}_1|^2 + \frac{2}{l_1\ C_1}\left(\sigma - l_1\bar{C}\right)^2\ |\tilde{Z}|^2 \tag{8}$$

And

$$\dot{V}_2 \leqslant -\frac{\mu}{2}|\tilde{Z}|^2 + \frac{2}{\mu}|P|^2\ |\bar{\bar{A}} - LC_1|^2\ |\tilde{X}_1|^2 \tag{9}$$

Now, combining (8) and (9) :

$$\dot{V} \leqslant -\beta|\tilde{Z}|^2 - \gamma|\tilde{X}_1|^2 \tag{10}$$

$$\beta = \left(\frac{\mu}{2} - \frac{2}{l_1\ C_1}\left(\sigma - l_1\bar{C}\right)^2\right) > 0 \tag{11}$$

$$\gamma = \left(l_1\frac{C_1}{2} - \sigma - \frac{2}{\mu}|P|^2\ |\bar{\bar{A}} - LC_1|^2\right) > 0 \tag{12}$$

We must ensure that the Lyapunov function derivative satisfies $\dot{V} < -\alpha V$, $\alpha > 0$ (then $\beta > 0$ and $\gamma > 0$) which guarantees exponential stability of the estimation error. To determine the gains, L is such that $(\bar{A} - L\bar{C})$ is Hurwitz and l_1 and L must satisfy inequalities (11-12)

Remark 1: In the case of the 2B continuous model, the linear part reduces to a scalar part. In this case, $Z = X_2$, $\phi_1 = \begin{bmatrix} A_{11} & A_{12}\end{bmatrix} X + B_1 u$, $\bar{A} = A_{22}$, $\bar{\bar{A}} = A_{21}$, $\bar{B} = B_2$, $\bar{C} = C_2$ and $L = l_2$.

This observer provides continuous state estimation assuming continuous availability of the output measurement.

■

B. Hybrid sampled-data observer with output prediction:

In practical implementations, measurements are only available at discrete instants t_k. Therefore, a sampled-data observer must be designed [19], [20]. Unlike classical ZOH-based observers, the proposed approach introduces an inter-sample output predictor that allows reconstructing the output between sampling instants.

More precisely, the observer operates as follows:

- For $t \in [t_k, t_{k+1})$, the observer evolves continuously using a predicted output $w(t)$.
- At each sampling instant t_k, the predictor is reset using the measured output:$w(t_k) = y(t_k)$

This mechanism ensures that the observer remains consistent with the measured output while providing continuous correction between sampling instants.

The observer equation (3) becomes :

$$\begin{cases} \dot{\hat{X}}_1(t) = \phi_1(\hat{X}(t), u(t)) + l_1(w(t) - \hat{y}(t)) \\ \dot{\hat{Z}}(t) = \bar{A}\hat{Z}(t) + \bar{\bar{A}}\hat{X}_1(t) + \bar{B}u(t) + L\,(w(t) - \hat{y}(t)) \\ \hat{Y}(t) = C_1\hat{X}_1(t) + \bar{C}\ \hat{Z}(t) + Du(t) \\ \dot{w}(t) = C_1(\phi_1(\hat{X}(t), u(t))) + \bar{C}(\bar{A}\hat{Z}(t) + \bar{\bar{A}}\hat{X}_1(t) \\ + \bar{B}u(t)) + D\dot{u}(t) - K(\hat{y}(t) - w(t)), t \in [t_k, t_{k+1}) \\ w(t_k) = y(t_k) \end{cases} \tag{13}$$

where $w(t)$ represents the predicted output between sampling instants, and K is a tuning gain that controls the convergence speed of the prediction error.

The predictor $w(t)$ plays a key role in the proposed approach, as it provides a continuous estimation of the output, unlike ZOH-based observers where the output is assumed constant between samples. Therefore, the observer is effectively corrected at each sampling instant using the measured output.

Theorem 3.2: There exists $T_{emax} > 0$, l_1 and a gain vector L such that, for $T_e \in (0, T_{emax})$, the hybrid observer (13) is exponentially convergent under Hypothesis 1.

Sketch of Proof:

The proof follows similar arguments to those used in Theorem 3.1. The extension to sampled-data observer comes from the application of the theorem 2.1 (main result, part 3) in [20], which guarantees exponential stability under sufficiently small sampling periods.

■

IV. Simulation and Results

In this section, the performance of the proposed hybrid observer is evaluated under realistic operating conditions using a WLTP current profile shown in Fig. 2a, for two representatives sampling times (0.02 s and 1 s).

A. Dynamic load profile

The WLTP driving cycle is adopted due to its highly dynamic nature, including strong acceleration and deceleration phases, high power demand, and abrupt current variations. These characteristics make it particularly challenging for sampled-data observers, as they amplify inter-sample errors.

The current profile is derived from experimental test-bench data reported in [21]. Although similar behaviors were observed using the NEDC cycle Fig. 2b, only WLTP results are presented here for clarity, as it represents more demanding and realistic operating conditions.

The analysis is restricted to the first 400 seconds of the cycle, where the most significant transients occur.

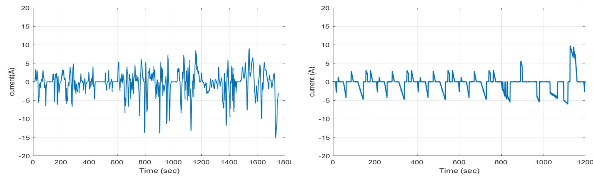

(a) WLTP (b) NEDC

Fig. 2. Current input profiles

B. hybrid nonlinear observer results

The parameters used in this study are summarized in Tab. I and are based on a widely accepted reference SC, a Maxwell BCAP 2.7V 1500F K2 series, commonly cited as a benchmark in the literature [9]. The system is initialized

nominal capacitance	$C_{rated} = 1500\ F$
nominal voltage	$U_n = 2.7\ V$
fast branch	$C_0 = 900\ F,\ C_v = 300\ F/V,$ $R_1 = 1.5\ m\Omega,$
interm. branch	$C_2 = 200\ F,\ R_2 = 0.4\ \Omega,$
slow branch	$C_3 = 330\ F,\ R_P = 4\ k\Omega$ $R_3 = 3.2\ \Omega,$

TABLE I

SUPERCAPACITOR 1500-F THREE-BRANCH PARAMETERS

at $[U_n\ 0\ 0]$, corresponding to a fully charged state, while the observer is initialized at $[U_n\ 0.01\ 0.01]$ to avoid numerical issues near zero. Despite this mismatch, the observer exhibits exponential convergence.

In our previous ZOH-based sampled observer, estimation peaks and delays were observed under fast-charging current profiles such as WLTP. These limitations are due to the fact that corrections are applied only at discrete sampling instants.

The proposed hybrid nonlinear observer overcomes this issue by introducing an inter-sample output predictor, allowing continuous correction between measurements and improving tracking accuracy during fast transients.

The sampling period is selected according to the fastest system dynamics. For the 3B model, the smallest time constant is approximately $\tau_{min} \approx 1s$, leading to the condition $T_e < \tau_{min}/3$. Two sampling periods are considered : $T_e = 0.02s$, corresponding to real-time embedded implementations and enabling comparison with previous results, and $T_e = 1s$, which exceeds the recommended bound and represents a constrained sampling scenario. In both cases, a moderate predictor gain $K = 10$ is used. The gain K adjusts the contribution of the predictor between samples, and is a key parameter in the observer's correction mechanism. The simulation results show that the hybrid observer significantly reduces estimation errors and eliminate the peaks observed in ZOH-based observers. Even for large sampling periods, the system remains stable and accurate.

Remark 2: The estimation error on the first state is significantly lower than that of the other states. This is explained by the fact that the first state corresponds to the fast dynamic branch, which is more directly influenced by the input and more strongly coupled to the measured output.

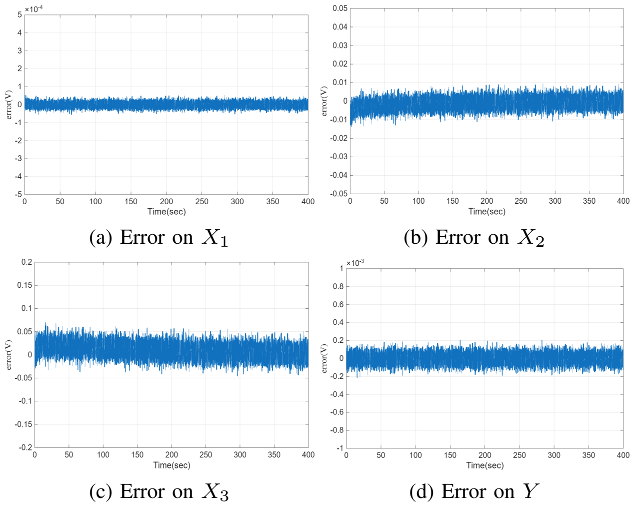

(a) Error on X_1 (b) Error on X_2

(c) Error on X_3 (d) Error on Y

Fig. 3. Estimation errors with WLTP input and $T_e = 0.02s$

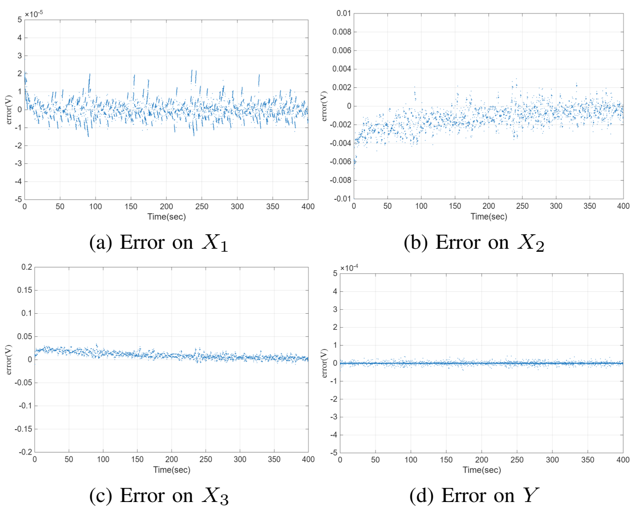

(a) Error on X_1 (b) Error on X_2

(c) Error on X_3 (d) Error on Y

Fig. 4. Estimation errors with WLTP input and $T_e = 1s$

Similar estimation behaviors were also observed under the NEDC cycle. Due to the smoother update mechanism, the amplitudes of the estimation error peaks are reduced by approximately 60% compared to the ZOH-based observer with $T_e = 0.02s$. In the same way, the convergence is slower with $T_e = 1s$.

1) SOC results: A method for calculating the SOC is presented in [14]. The definition of SOC raises several considerations, as discussed in [22]. SOC could be defined as the ratio between the actual charge Q and the nominal charge Q_n (obtained through manufacturer nominal parameters such as maximal initial capacitance and rated voltage [23]). Based on the structure of our model, SOC can be expressed as :

$$SOC = \frac{Q}{Q_n} = \frac{(C_0 + C_v V_{c_1})V_{c_1} + C_2 V_{c_2} + C_3 V_{c_3}}{Q_n} \tag{14}$$

Accurate estimation of internal voltages is therefore essential for reliable SOC estimation. Simulation results Fig . 5 show that the SOC estimation error remains within the order of 10^{-3}, even under dynamic load conditions. The hybrid observer provides stable and smooth estimation, with reduced

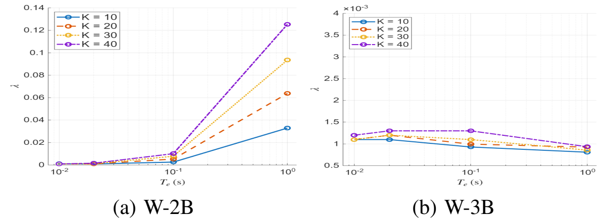

(a) W-2B (b) W-3B

Fig. 6. RMSE metric λ for SOC with WLTP (a,b) inputs

fluctuations during transient phases. Although slightly lower errors are observed for $T_e = 1$s, this effect is mainly due to the reduced number of data points, which smooths the error curve. In practice, the convergence is slower for larger sampling periods. Overall, SOC estimation remains consistent for both sampling periods, confirming the robustness of the proposed observer.

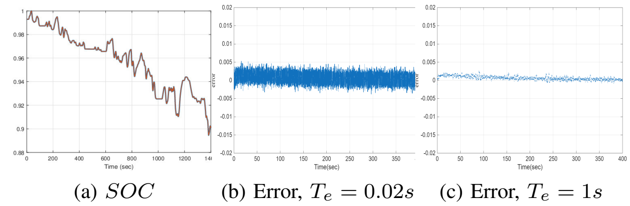

(a) SOC (b) Error, $T_e = 0.02s$ (c) Error, $T_e = 1s$

Fig. 5. SOC and errors for hybrid nonlinear observer with WLTP input

2) Quantitative Comparison: RMSE-Based Evaluation: To quantitatively evaluate the performance in both case, we compute λ, a Root Mean Square Error (RMSE) between the estimated SOC and the reference SOC obtained from the model. The RMSE is a standard metric that reflects the average magnitude of estimation errors and is defined as:

$$\lambda = \sqrt{\frac{1}{N}\sum_{k=1}^{N}\left(SOC_k - \widehat{SOC}_k\right)^2} \tag{15}$$

Where SOC_k is the true value at time step k, and $\widehat{SOC}$ is the SOC estimated by the observer at the same time step. In this study, λ values are computed for various combinations of sampling periods $T_e \in \{0.01s \quad 0.02s \quad 0.1s \quad 1s\}$ and prediction gains $K \in \{0 \ 10 \ 20 \ 30 \ 40\}$ for both the 2B and 3B models.

Results Fig. 6 show that results are better with 3B model rather than the 2B, with lower RMSE values across all configurations. Increasing K improves convergence speed but may slightly degrade accuracy due to increased sensitivity to noise, highlighting a trade-off between responsiveness and robustness.

3) Discussion: The results demonstrate that :

- The hybrid observer significantly improves estimation accuracy compared to ZOH-based approaches.
- Inter-sample output prediction is essential under fast dynamics
- The proposed observer remains robust even for large sampling periods

Remark 3: The proposed observer may not outperform UKF-based methods for very small sampling periods. However, UKF performance typically requires high sampling rates ($T_e \approx 0.1s$), whereas the proposed method remains stable and effective over a wider range of sampling conditions. In addition, compared to EKF- and UKF-based approaches, the proposed observer does not require covariance matrix propagation or matrix inversion operations. This significantly reduces the computation burden and makes the proposed approach particularly suitable for embedded real-time implementation.

Remark 4: Further performance improvements could be achieved by optimizing the observer gains. However, this is beyond the scope of the present study.

V. Conclusion

In this paper, a hybrid continuous-discrete nonlinear observer with inter-sample output prediction has been proposed for SOC estimation of SCs. The proposed approach combines continuous-time prediction with discrete -time correction, allowing accurate estimation despite the sampled nature of the measurements. The introduction of an output predictor enables continuous correction between sampling instants, significantly improving estimation accuracy under fast-varying operating conditions.

Simulation results based on realistic driving cycles such as WLTP demonstrate the effectiveness of the proposed observer in reducing the estimation errors, improving robustness to large sampling periods, and maintaining good performance under dynamic load conditions.

Using a 3B models improve SOC estimation accuracy. From an implementation perspective, the proposed observer remains computationally efficient and suitable for real-time embedded applications. Future work will focus on experimental validation and optimization of the observer gains, as well as in-depth comparison with Kalman approaches.

Acknowledgment

This work is supported by SEGULA Technologies, 9 av. E. Belin, 92 500 Rueil Malmaison, FR. Thanks for their collaboration and financial support.

References

[1] A. El Mejdoubi, A. Oukaour, H. Chaoui, Y. Slamani, J. Sabor, and H. Gualous, "Online supercapacitor diagnosis for electric vehicle applications," *IEEE Trans. Veh. Technol.*, vol. 65, no. 6, pp. 4241–4252, 2015, doi:10.1109/TVT.2015.2454520.

[2] J. T. J. Burd, E. A. Moore, H. Ezzat, R. Kirchain, and R. Roth, "Improvements in electric vehicle battery technology influence vehicle lightweighting and material substitution decisions," *Appl. Energy*, vol. 283, p. 116269, 2021, doi:10.1016/j.apenergy.2020.116269.

[3] S. M. Lukic, S. G. Wirasingha, F. Rodriguez, J. Cao, and A. Emadi, "Power management of an ultracapacitor/battery hybrid energy storage system in an hev," in *IEEE VPPC*, Windsor, UK, 2006, pp. 1–6, doi:10.1109/VPPC.2006.364357.

[4] J. Cao and A. Emadi, "A new battery/ultracapacitor hybrid energy storage system for electric, hybrid, and plug-in hybrid electric vehicles." *IEEE Trans. Power Electron.*, vol. 27, no. 1, pp. 122–132, 2011, doi:10.1109/TPEL.2011.2151206.

[5] J. Park, B. Raju, and A. Emadi, "Effects of an ultra-capacitor and battery energy storage system in a hybrid electric vehicle," SAE International, Technical Paper 2005-01-3452, 2005, doi:10.4271/2005-01-3452.

[6] S. Fan, J. Duan, L. Sun, K. Zhang, and Y. Han, "State of charge estimate for super-capacitor based on sliding mode observer," in *ITEC, Asia-Pacific*, Harbin, China, 2017, pp. 1–5, doi:10.1109/ITEC-AP.2017.8080946.

[7] F. Naseri, E. Farjah, Z. Kazemi, E. Schaltz, T. Ghanbari, and J.-L. Schanen, "Dynamic stabilization of DC traction systems using a supercapacitor-based active stabilizer with model predictive control," *IEEE Trans. Transp. Electrif.*, vol. 6, no. 1, pp. 228–240, 2020, doi:10.1109/TTE.2020.2967257.

[8] A. Ayob, S. Ansari, M. S. H. Lipu, A. Hussain, and M. H. M. Saad, "SOC, SOH and RUL estimation for supercapacitor management system: Methods, implementation factors, limitations and future research improvements," *Batteries*, vol. 8, no. 10, p. 189, 2022, doi:10.3390/batteries8100189.

[9] L. Zubeita and R. Bonert, "Characterization of double-layer capacitors of power electronics applications," *IEEE Trans. Ind. Appl.*, vol. 36, no. 1, pp. 199–205, 2000, doi:10.1109/28.821816.

[10] Y. Zhou, Z. Huang, H. Li, J. Peng, W. Liu, and H. Liao, "A generalized extended state observer for supercapacitor state of energy estimation with online identified model," *IEEE Access*, vol. 6, pp. 27 706 – 27 716, 2018, doi:10.1109/ACCESS.2018.2837036.

[11] Z. Lei, W. Zhenpo, H. Xiaosang, and D. G. Dorrell, "Residual capacity estimation for ultracapacitors in electric vehicles using artificial neural network," *IFAC Proceedings Volumes*, vol. 47, no. 3, pp. 3899–3904, 2014, doi:10.3182/20140824-6-za-1003.00657.

[12] A. Nadeau, G. Sharma, and T. Soyata, "State-of-charge estimation for supercapacitors : A kalman filtering formulation," in *ICASSP*, Firenze, Italia, 2014, pp. 2194–2198, doi:10.1109/ICASSP.2014.6853988.

[13] A. Nadeau, M. Hassanalieragh, G. Sharma, and T. Soyata, "Energy awareness for supercapacitors using kalman filter state-of-charge tracking," *J. Power Sources*, vol. 296, pp. 383–391, 2015, doi:10.1016/j.jpowsour.2015.07.050.

[14] H. El Fadil, F. Z. Belhaj, A. Rachid, F. Giri, and T. Ahmed-Ali, "Nonlinear modeling and observer for supercapacitors in electric vehicle applications," *IFAC Hosting by Elsevier Ltd*, 2017, doi:10.1016/j.ifacol.2017.08.262.

[15] F. Naseri, S. Karimi, E. Farjah, E. Schaltz, and T. Ghanbari, "Co-estimation of supercapacitor states and parameters considering three-branch equivalent circuit model," in *11th PEDSTC*, Teheran, Iran, 2020, doi:10.1109/PEDSTC49159.2020.9088356.

[16] I. Belghazi, E. Magarotto, T. Ahmed-Ali, and M. Haddad, "A sampled observer for a three-branch supercapacitor model: voltages estimation for SOC under NEDC and WLTP cycles," in *11th IEEE CODIT, Split, Croatia,*, 2025, pp. 1001–1006, doi: 10.1109/CoDIT66093.2025.11321728.

[17] J. Chen, H. Chen, M. Zhou, L. Kumar, and J. Zheng, "Quadratic programming-based simultaneous charging strategy for battery packs of electric vehicles," *IEEE/ASME Transactions on Mechatronics*, vol. 27, no. 6, 2022, doi:10.1109/TMECH.2022.3190326.

[18] Z. Cabrane and S. Lee, "Electrical and mathematical modeling of supercapacitors: Comparison," *Energies*, vol. 15, no. 3, 2022, doi:10.3390/en15030693.

[19] I. Karafyllis and C. Kravaris, "From continuous-time design to sampled-data design of observers," *IEEE Trans. Autom. Control*, vol. 54, no. 9, pp. 2169–2174, 2009, doi:10.1109/TAC.2009.2024390.

[20] I. Karafyllis, T. Ahmed-Ali, and F. Giri, "A note on sampled-data observers," *Syst. Control Lett.*, vol. 144, p. 104760, 2020, doi: 101016/j.sysconle.2020.104760.

[21] E. Magarotto, J.-F. Massieu, P. Dorléans, and A. Oukaour, "A new observer design for aging detection of supercapacitors," *J. Dyn. Syst. Meas. Contr.*, vol. 141, no. 4, p. 041004, 12 2018, doi:10.1115/1.4041812.

[22] N. Watrin, B. Blunier, and A. Miraoui, "Review of adaptive systems for lithium batteries state-of-charge and state-of-health estimation," in *ITEC*, Dearborn, MI, USA, 2012, pp. 1–6, doi:10.1109/ITEC.2012.6243437.

[23] BCAP1500 P270, *Maxwell_K2Series_DS_1015370–4–1179730.pdf*, Maxwell Technologies, 2021.